Improved energy storage and electrocaloric properties of lead-free $Ba_{0.85}Ca_{0.15}Zr_{0.1}Ti_{0.9}O_3$ ceramic

Afaak Lakouader[1,2,*] [ID], Hanane Mezzourh[1,2], Daoud Mezzane[1,2], M'barek Amjoud[1], Lahoucine Hajji[1], El Hassan Choukri[1], Igor A. Luk'yanchuk[2,3], Zdravko Kutnjak[4], and Mimoun El Marssi[2]

[1] IMED-Lab, Cadi Ayyad University, 40000 Marrakesh, Morocco

[2] LPMC, University of Picardy Jules Verne, 80039 Amiens, France

[3] Department of Building Materials, Kyiv National University of Construction and Architecture, Kiev 03680, Ukraine

[4] Jozef Stefan Institute, Jamova Cesta 39, 1000 Ljubljana, Slovenia

ABSTRACT

Lead-free $Ba_{0.85}Ca_{0.15}Zr_{0.1}Ti_{0.9}O_3$ (BCZT) ceramic powders were synthesized using the sol–gel method. The ceramics thickness was reduced to achieve high-energy storage and large electrocaloric effect in bulk ceramics. Dielectric, ferroelectric, energy storage, and electrocaloric properties were investigated for BCZT ceramic with 400 μm. Here, pure crystalline structure and homogenous microstructure were identified by XRD analysis and SEM measurements, respectively. The dielectric measurements revealed a maximum dielectric constant associated with ferroelectric–paraelectric phase transition. The maximum of ε'_r was 17841, around 352 K. Furthermore, the BCZT ceramic exhibited improved energy storage and electrocaloric properties. A high recoverable energy density W_{rec} of 0.24 J/cm³ and a total energy density W_{total} of 0.27 J/cm³ with an efficiency coefficient of ∼ 88% at 423 K under an electric field of 55 kV/cm were obtained. Besides, The maximum value of ΔT = 2.32 K, the electrocaloric responsivity ζ = 0.42 K mm/kV, the refrigeration capacity RC = 4.59 J/kg and the coefficient of performance COP = 12.38 were achieved around 384 K under 55 kV/cm. The total energy density W_{total} and the temperature change ΔT were also calculated by exploiting the Landau–Ginzburg–Devonshire (LGD) theory. The theoretical results matched the experimental findings. These results suggest that the synthesized BCZT ceramic with reduced thickness could be a promising candidate for energy storage and electrocaloric applications.

Address correspondence to E-mail: afaak.lakouader@gmail.com

🍊 Springer

1 Introduction

Ferroelectric materials can be defined as dielectric materials in which permanent polarization exists even after removing the applied electric field. For most applications of ferroelectric materials, the dielectric constant and loss are essential practical parameters. These applications include non-volatile memories, pyroelectric detectors, sensors, actuators, transducers, capacitors, generators, optical memories, and energy harvesting devices [1].

The most used ferroelectric materials are oxides with a perovskite structure of ABO_3. A cubic lattice of space group (Pm-$3m$) describes this high symmetry structure [2]. Where A is an alkali cation, alkaline earth, or rare-earth, B is a transition cation of atomic radius smaller than that of site A. The structure is a network of corner-linked oxygen octahedral, with the smaller cation filling the octahedral holes and the large cation filling the dodecahedral holes.

Among perovskite ferroelectric materials, the most studied are lead titanate ($PbTiO_3$) [3], lead zirconate titanate (PZT) [4], lanthanum zirconate titanate (PLZT) [5]. However, lead is recognized as toxic, dangerous to humans and the environment. Therefore, it is necessary to develop environmentally friendly materials with no lead [6]. Thus, several scientific works have focused mainly on $BaTiO_3$ (BT) perovskite because it has interesting advantages such as low dielectric loss and stable electrical properties for long-term operations [7]. However, their use is limited due to their relatively high curie temperature T_c ($\sim$ 390 K) [8]. Therefore, adequate atomic substitutions are expected to modify the chemical bonds of the structure and, thus, the mobility of the ions and the resulting polarizability. A series of studies have been initiated to modify the dielectric and ferroelectric properties of $BaTiO_3$ systems, including $(Ba,Ca)TiO_3$ [9], $Ba(Ti,Zr)O_3$ [10], $(Ba,Ca)(Ti,Sn)O_3$ [11], etc. In these doped (BT) matrix systems, the dielectric loss of $Ba(Ti,Zr)O_3$(BZT) ceramics is very low, which can be attributed to the increased substitution rate of zirconium [12]. In addition, the good temperature stability of (Ba, Ca) TiO_3 (BCT) ceramics is due to the introduction of Ca at site A of the BT system, which leads to the diffuse phase transition [13].

More recently, $(Ba,Ca)(Zr,Ti)O_3$ (BCZT) materials with Ca^{2+} and Zr^{4+} at site A and site B of the $BaTiO_3$ perovskite structure have been widely studied for their excellent dielectric, ferroelectric and piezoelectric properties, and their composition closed to the morphotropic phase boundary MPB [14]. Among these ceramics, $xBa (Zr_{0.2}Ti_{0.8}) O_3^- (1 - x) (Ba_{0.7}Ca_{0.3})$ TiO3 ceramics with $(0.48 < x < 0.52)$ were largely studied, and the results showed that the composition $Ba_{0.85}Ca_{0.15}Zr_{0.1}Ti_{0.9}O_3$ has considerable dielectric, ferroelectric and piezoelectric properties compared to other components [15]. In this regard, Wang et al. reported that $Ba_{0.85}Ca_{0.15}Zr_{0.1}Ti_{0.9}O_3$ ceramics exhibit a high spontaneous polarization (P_s = 9.69 $\mu C/cm^2$), a low coercive field (E_c = 1.89 kV/cm) and a high-dielectric permittivity (ε_r' = 16,310) [16]. In addition, due to low-remnant polarization, high-maximal polarization, and adjustable breakdown strength (BDS), relaxor ferroelectrics (RFEs), including BCZT, have a promising future in the field of dielectric energy, and their electric polarization response can be converted into recoverable electrostatic energy.

One of the crucial aspects of functional microstructure is the synthesis method. Many papers have reported that the sol–gel process should be a rather promising approach as it offers the possibility of mixing metal ions at the atomic level [17, 18]. Besides, this method also has several potential advantages of better homogeneity, chemical purity, and stoichiometric composition, which can be difficult to achieve by the solid-state method [19]. With a variation of the sintering temperature, various BCZT properties can be extracted. Ji et al. reported that BCZT sintered at 1400 °C had a uniform microstructure with a density of 5.56 g/cm^3 and had excellent electrical properties (ε_r' = 8808, P_r = 12.24 $\mu C/cm^2$, d_{33} = 485 pC/N) [20]. Moreover, BCZT ceramics obtained by sol–gel method and sintered at 1420 °C have outstanding electrical and energy storage properties (d_{33} = 558 pC/N, ε_r' = 3375, $tg\delta$ = 0.02, and W = 0.52 J/cm^3) as evaluated by Zhong Ming Wang et al. [17]. The energy density can also be demonstrated by exploiting the Landau-Ginzburg-Devonshire (LGD) phenomenological theory. The modelling result supports the experimental findings as reported for $BaTiO_3$-$BaSnO_3$ by Yonggang et al. [21].

Moreover, the electrocaloric effect could be investigated by indirect EC effect calculation through Maxwell relation and theoretical investigations based on the phenomenological approach via Landau–Ginzburg–Devonshire (LGD) theory. Meanwhile, a large electrocaloric responsivity ($\xi = \Delta T/\Delta E$) was

found (ξ = 0.19 K mm/kV) for BCZT ceramic sintered at 1420° C, as reported by Kaddoussi et al. [22]. Additional estimations of the EC effect in ferroelectric materials can be obtained by theoretical investigations exploiting the LGD phenomenological approach.

A different approach has been used to improve the electrocaloric efficiency (1) by monitoring the perovskite composition, (2) by combining ferroelectric, relaxor ferroelectric, and antiferroelectric materials, (3) using composites (ceramics/polymers), and (4) by reducing the ceramic thickness. On the other hand, according to previous studies on the energy storage density of material dielectrics, a higher breakdown strength is responsible for a larger energy storage density [23]. In this regard, the breakdown strength of dielectrics increases exponentially with decreasing ceramic thickness [24]. Thus, reducing thickness is a practical method to enhance dielectrics' breakdown strength and energy density. As a result, the dielectric thin films exhibit high breakdown strength, large energy storage density and giant electrocaloric effect compared to bulk ceramics. However, their energy capacities are low because of the low thickness or volume of thin films, making them unsuitable for cooling applications where a high level of energy is needed. This indicates that thin bulk ceramics should be more appropriate for practical energy storage density and electrocaloric effect. Thus, to achieve higher energy storage properties and a giant electrocaloric effect in bulk ceramics, enhancing the breakdown strength is necessary to tolerate strong electric fields while keeping a large dielectric volume. This can be accomplished by decreasing the ceramic's thickness.

This work aims to improve the energy storage and electrocaloric properties of BCZT ceramic prepared by the sol–gel method while reducing its thickness. The energy storage properties were determined from the *P–E* hysteresis and the experimental findings were compared with the theoretical results derived from the phenomenological approach through the LGD theory. Furthermore, the electrocaloric effect was investigated by two methods: the indirect approach following Maxwell's relation and the phenomenological approach through the LGD theory.

2 Experimental

The $Ba_{0.85}Ca_{0.15}Zr_{0.1}Ti_{0.9}O_3$ ceramic was synthesized by the sol–gel route. Stoichiometric amounts of barium acetate $Ba(CH_3COO)_2$ (99%), calcium nitrate tetrahydrate $Ca(NO_3)_2 \cdot 4H_2O$ (99%), zirconyl chloride octahydrate $ZrOCl_2.8H_2O$ (98%), and titanium isopropylate $C_{12}H_{28}O_4Ti$ (97%) were used as precursors. As solvents, acetic acid (100%) and 2-methoxyethanol (99%) were chosen. $Ba(CH_3COO)_2$ and $Ca(NO_3)_2 \cdot 4H_2O$ were initially dissolved in acetic acid, while $[ZrOCl_2 \cdot 8H_2O]$ was dissolved in 2-Methoxyethanol, then an appropriate amount of $C_{12}H_{28}O_4Ti$ was added. The precursor solution of (Zr,Ti) was added to that of (Ba,Ca) and stirred for 1 h at room temperature to give a BCZT solution, and then the pH was adjusted with ammonia to 7. The sol obtained was dried in air for 48 h to remove the solvents and then ground into a fine powder in a mortar. The powder was calcined for 4 h at 1000° C in the air to form a pure crystalline phase. The calcined powder was then pressed into cylindrical discs by uniaxial pressing to prepare pellets sintered at a high temperature of 1420° C for 4 h to improve the ceramic's density. The pellets were polished to adjust the ceramic thickness at 400 μm.

The sintered ceramic's phase structure was determined by X-ray diffraction (XRD, Panalytical X-Pert Pro) analysis using the Cu-Kα radiation with $\lambda \sim 1.540598$ Å. The measurements were performed at room temperature in a range of 2θ from 20° to 80° with a step size of 0.02°. Rietveld refinement analysis was realized using FullProf software. A Scanning Electron Microscope (SEM, VEGA 3-Tscan) revealed the surface's morphologies. The density of the pellet was measured using Archimedes' method. The dielectric measurements were examined using an HP 4284A precision impedance meter, controlled by a computer in the 20 Hz to 1 MHz frequency range. Differential scanning calorimetry (Perkin–Elmer Jade DSC) with a heating rate of 5 °C/min was utilized to highlight the various phase transitions. The surfaces of the sintered sample were covered with a conductive silver paste serving as electrodes for electrical measurements. The polarization–electric field (*P–E*) hysteresis loops were collected using CPE1701, PolyK, USA, with a high-voltage power supply (Trek 609–6, USA). The electrocaloric study was achieved by the indirect method from recorded (*P–E*) hysteresis loops at 10 Hz as a function of temperature.

3 Results and discussion

### 3.1 Structural and microstructural properties

Figure 1 presents the X-ray diffraction pattern of BCZT ceramic sintered at 1420 °C for 4 h. The formation of a complete single-phase perovskite structure, with any impurity phase, is evident in the room temperature XRD data, suggesting that Ca^{2+} and Zr^{4+} have been diffused into the $BaTiO_3$ lattice to form a solid solution [25]. The peak between $2\theta \approx 45°$ was split into two peaks corresponding to (002) and (200) planes, as represented in Fig. 1b. This could be the reflection of a tetragonal structure [26]. The splitting peaks of (022) and (200) around $2\theta \approx 45°$ imply the existence of an orthorhombic phase which can also be confirmed by the formation of the triplet around $2\theta \approx 66°$ [27], as displayed in Fig. 1c. The coexistence of orthorhombic and tetragonal phases indicates the formation of BCZT ceramic at the morphotropic phase boundary (MPB). The coexistence of tetragonal and orthorhombic phases at room temperature was also reported in many reports [16, 28]. The data of XRD was analyzed by Rietveld refinement [29, 30], which was achieved using a combination of tetragonal symmetry with space group $P4mm$ and orthorhombic symmetry with space group $Pmm2$ ($\chi^2 = 1.86$, $R_p = 17.1$ and $R_{wp} = 13.5$). Structural information and phase composition are regrouped in Table 1.

Figure 2 shows the surface morphology of the sample of the BCZT ceramic sintered at 1420 °C. The grains of the ceramic show an irregular morphology and a uniform distribution. The average grain size is 45 μm. The SEM shows that the ceramic displays a dense morphology due to the high-sintering temperature. The latter facilitates the mass transfer and pore removal resulting in tightly packed grains and a high density of 5.70 g/cm^3, which is ∼ 95% of the theoretical density.

3.2 Dielectric properties

Figure 3a shows the thermal variations of the real part of the dielectric permittivity (ε'_r) as a function of the frequency for BCZT ceramic; the inset shows the dielectric losses ($tg\delta$). The results show that ε'_r increases rapidly and then decreases with increasing measurement temperature. This behavior is the same as a conventional ferroelectric material [31]. Two dielectric anomalies, T_{O-T} and T_C, were observed
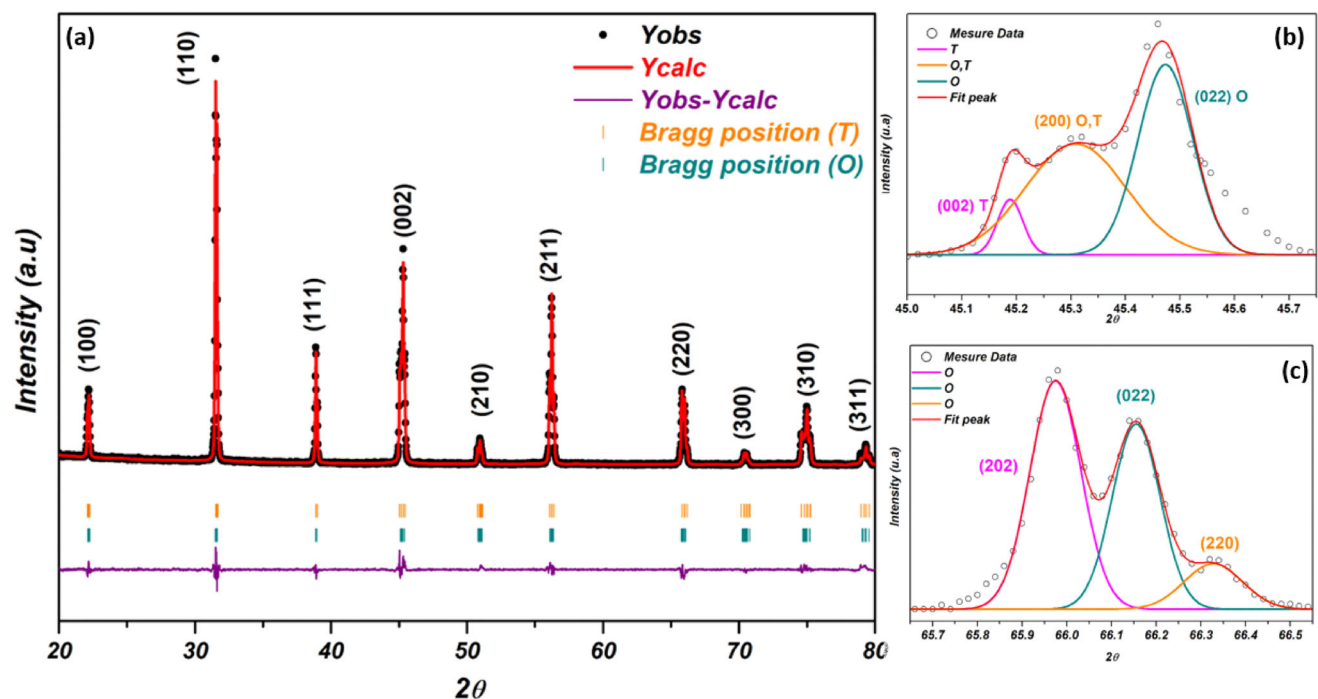

Fig. 1 **a** XRD patterns and Rietveld refinement of BCZT sample sintered at 1420 °C for 4 h, **b** XRD patterns for 2θ between [45° and 46°], **c** XRD patterns for 2θ between [65° and 67°]

Table 1 Structural parameters, average crystalline size, and relative density of BCZT ceramic

Structure		Tetragonal				Orthorhombic		
Space group		P4mm				Pmm2		
Unit cell parameters	a (Å)	3.999900				4.001126		
	b (Å)	3.999900				4.016704		
	c (Å)	4.022146				4.011608		
	$\alpha = \beta = \delta$	90°				90°		
Volume ($\mathring{A}^3$)		64.35				64.47		
(c/a)		1.005						
Phase composition (wt%)		66.51				33.49		
Reliability factors (%)	χ^2			1.86				
	R_p			17.1				
	R_{wp}			13.5				
		x	y	z		x	y	z
Atomic position	Ba/Ca	0.00000	0.00000	− 0.01573		0.00000	0.00000	0.03760
	Ti/Zr	0.50000	0.50000	0.46531		0.50000	0.50000	0.46350
	O1	0.50000	0.00000	0.41492		0.50000	0.00000	0.84859
	O2	0.50000	0.50000	0.06960		0.50000	0.05000	0.61207
	O3	–	–	–		0.00000	0.50000	0.64283
Average grain size (μm) by SEM				45				
Relative density (%)				95				
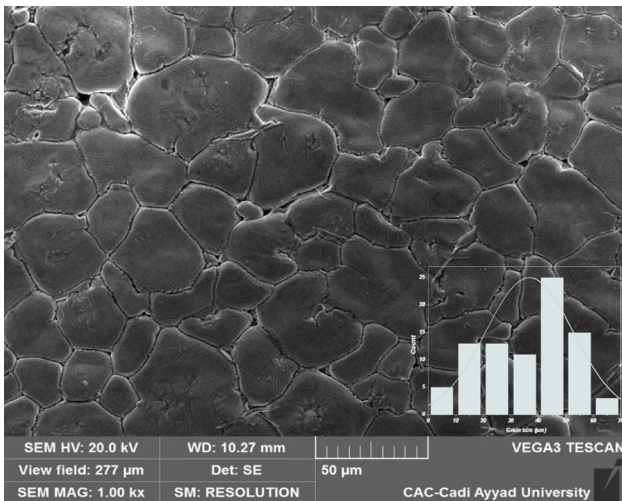
**Fig. 2** The SEM image of sintered BCZT ceramic sintered at 1420 °C

around 300 and 352 K, corresponding to the phase transitions from orthorhombic to tetragonal and tetragonal to cubic, respectively. This result agrees well with DSC data, revealing two endothermic peaks at the same transition temperature ($T_{O–T}$ and T_C) (Fig. 3b). The response of space charge polarization induced by the creation of lattice vacancies, such as cation or oxygen vacancies, could cause a high ε'_r at a low frequency [26]. However, as frequency increases, space charge polarization become more limited, resulting in a decrease in ε'_r [26]. At 1 kHz, the maximum of ε'_r was 17,841 around 352 K. The dielectric loss $tg\delta$ was less than 0.06, which may be attributed to the dense microstructure and the lower electron diffusion in the grain boundaries [33]. Compared to BCZT synthesis by solid-state and sintered at 1350 °C, the maximum of ε'_r was 6330 around 388 K [32], which is lower than our results. The increase in ε'_r could be caused by increasing density, which is essential for the electrocaloric effect.
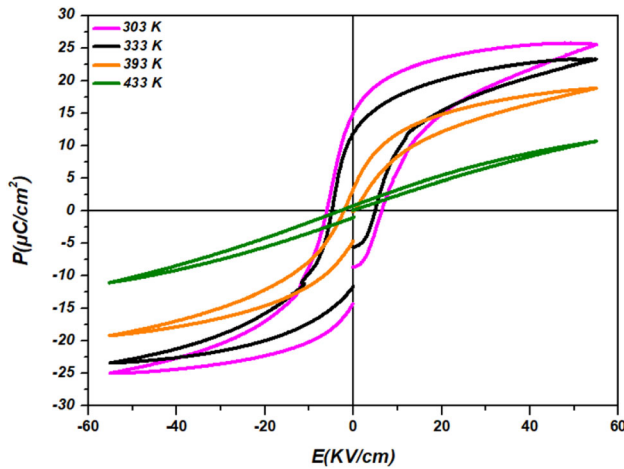
3.3 Ferroelectric properties

Figure 4 show the hysteresis loops at different temperatures at an electric field of 55 kV/cm for BCZT ceramic. The measurements were carried out at different temperatures and at a constant frequency of 10 Hz. At 303 K, the P–E loop reveals a closed and saturated loop similar to a conventional ferroelectric behavior [33]. The maximal polarization (P_{max}) was 25.75 μC/cm^2, the remnant polarization (P_r) was 15.15 μC/cm^2, and the coercive field (E_c) was found to be 6.41 kV/cm. It is also observed that the hysteresis loops showed typical characteristics of ferroelectric to paraelectric phase transition with nonlinear to linear behavior [34]. As the temperature increases,

Fig. 3 a Temperature variation of dielectric properties at different frequencies of BCZT sample; inset: dielectric loss at different frequencies, b DSC heat flow of BCZT with a heating rate of 5 °C/min
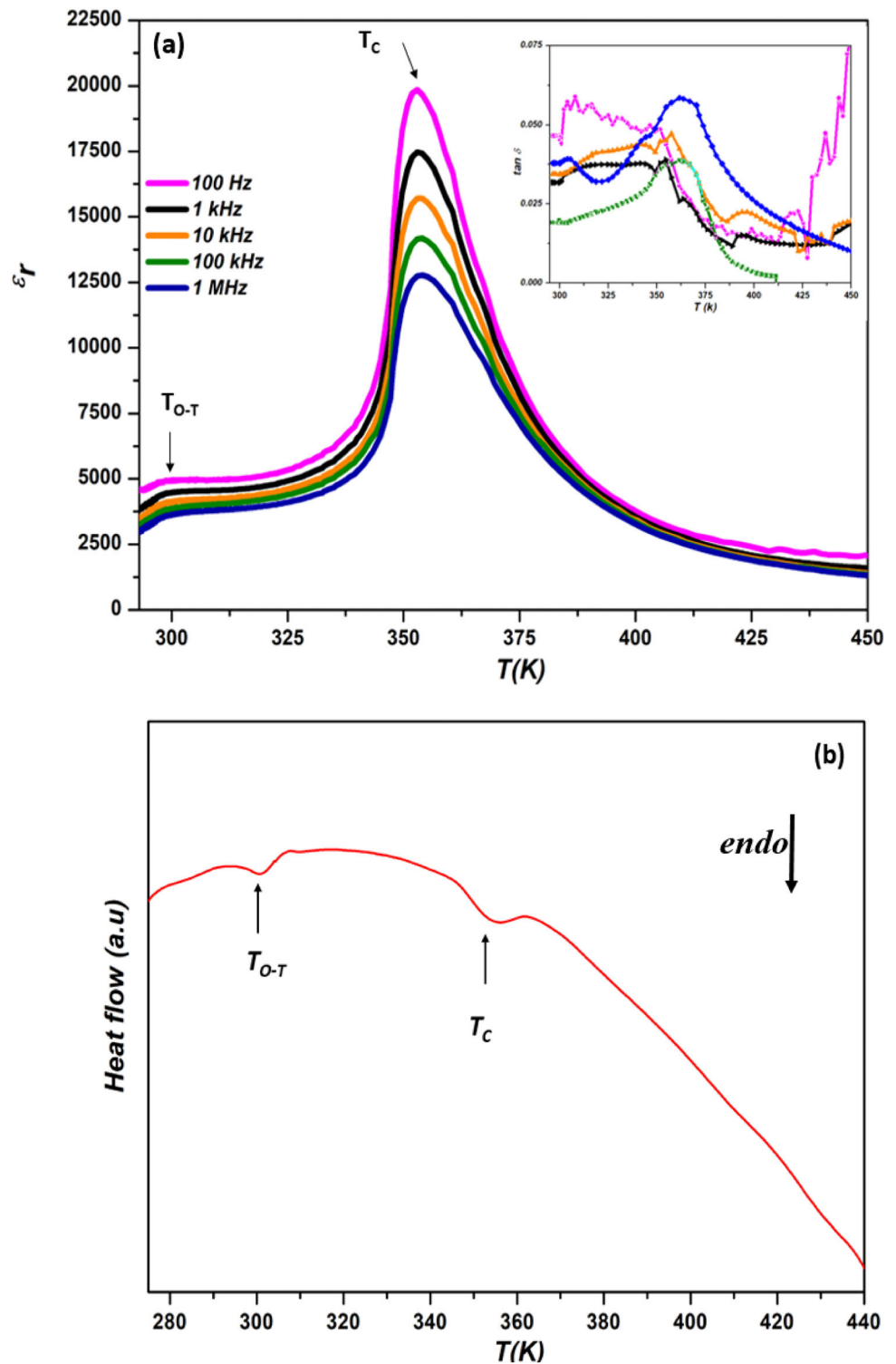
the hysteresis loops narrow until linear behavior is achieved, and there is a continuous decrease of P_r, E_c, and P_{max} due to the thermal agitation [35]. This behavior is a typical feature of paraelectric ferroelectric phase transitions. P_r and P_{max}'s value is higher than that of BCZT ceramic prepared by solid-state reaction ($P_{max} = 16.01$ μC/cm^2–$P_r = 10.98$ μC/cm^2) [32] due to a good homogeneity in grain size and uniform grain microstructure of the samples prepared by sol–gel. Indeed, the proportion (f) of

Fig. 4 The hysteresis loops at different temperatures at an electric field of 55 kV/cm for BCZT ceramic

Fig. 5 *P–E* curve with a schematic for calculating energy storage performance

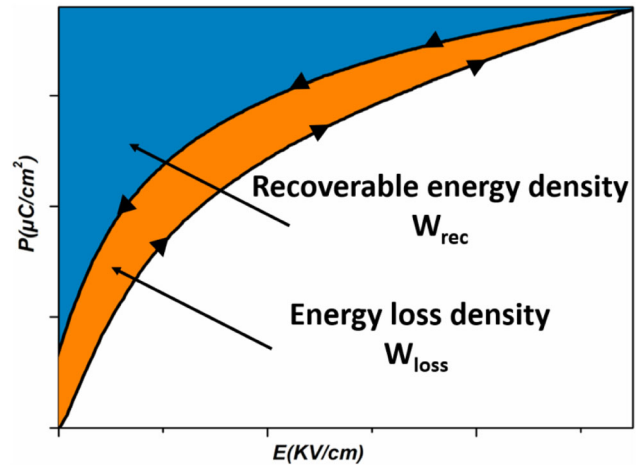grains' contribution to polarization for ferroelectric materials can be described by [36]:

$$f = f_0 \left[1 - \exp\left(\frac{-G_a d^3}{kT}\right) \right] \quad (1)$$

where d is the grain size and G_a is a constant representing the grain anisotropy energy density. Therefore, the ferroelectric properties were proportional to grain size. Thus, with the increasing grain size, the contribution of grain to polarization increases, giving rise to the enhancement of ferroelectricity [36]. Besides, a relatively lower E_c was found compared to ceramic prepared by solid-state ($E_c = 9.30$ kV/cm) [32]. The large grain of ferroelectric ceramics is beneficial to a fast ferroelectric domain switching resulting in a reduced coercive electric field.

3.4 Energy storage performances

The energy storage properties of BCZT ceramic were deduced from the *P–E* hysteresis loops as a function of temperature. Nonlinear dielectrics possess some energy dissipation. Therefore, the total energy density (W_{total}), recoverable energy density (W_{rec}), and energy storage efficiency (η) could be calculated using the equations [37]:

$$W_{total} = \int_0^{P_{max}} E \, dP \quad (2)$$

$$W_{rec} = \int_{P_r}^{P_{max}} E \, dP \quad (3)$$

$$\eta = \frac{W_{rec}}{W_{total}} \times 100 \quad (4)$$

P–E loops' upper and lower branches represent the discharge and charge process, respectively. W_{rec} could be determined by integrating the area between the polarization axis and the upper branch curve of the unipolar *P–E* hysteresis loop, W_{rec} represents the energy released during the discharging process. In contrast, W_{loss} produced by the domain reorientation is determined by integrating the P–E loop area and corresponds to the dissipation in dielectrics. W_{total} can be calculated by adding W_{rec} and W_{loss} as schematically presented in Fig. 5, and it corresponds to the total energy density during the charging process.

## 3.5 Electric-field-dependent energy storage properties at room temperature

Using Eqs. (2–4), the obtained values of total energy density W_{total}, energy storage density W_{rec}, energy loss density W_{loss}, and energy storage efficiency η as a function of electric field have been illustrated in Fig. 6. W_{total}, W_{rec}, and W_{loss} display a sharp linear rise with the increasing applied electric field at room temperature. W_{total}, W_{rec}, and W_{loss} increased from 0.10 to 0.55 J/cm^3, 0.01 to 0.12 J/cm^3 and 0.08 to

Fig. 6 Total energy density (W_{total}), energy storage density (W_{rec}), energy loss density (W_{loss}), and energy storage efficiency η as a function of the electric field at room temperature for BCZT ceramic
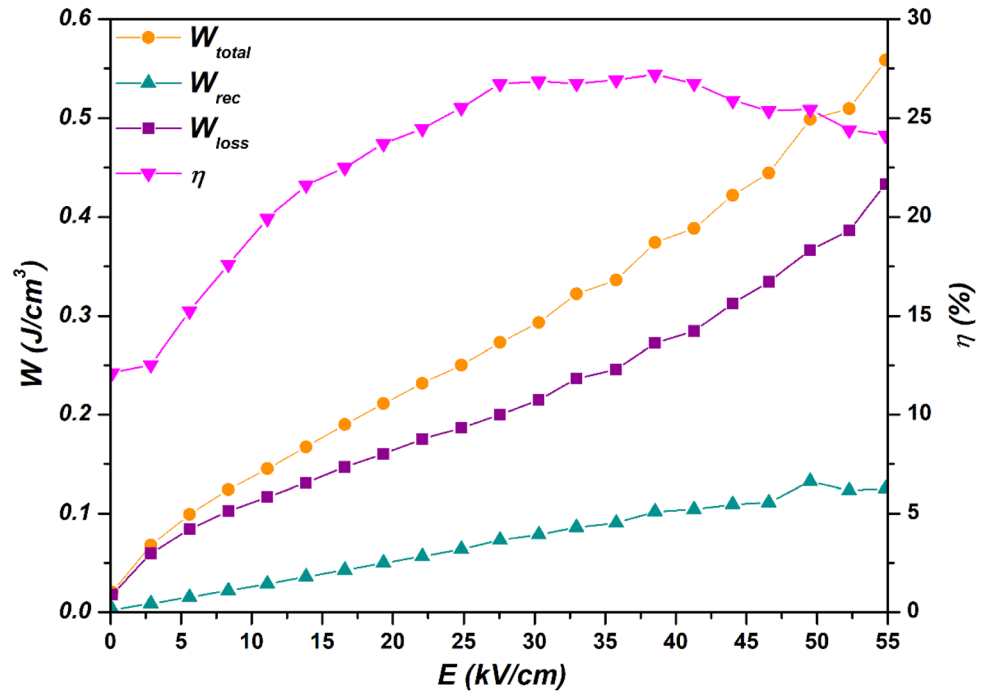
Fig. 7 Total energy density (W_{total}), energy storage density (W_{rec}), energy loss density (W_{loss}), and energy storage efficiency (η) as a function of temperature for BCZT ceramic at 55 kV/cm Fig. 8 Comparison of the thermal evolution of W_{total} obtained experimentally and using Landau–Ginzburg–Devonshire (LGD) theory at 55 kV/cm for BCZT ceramic
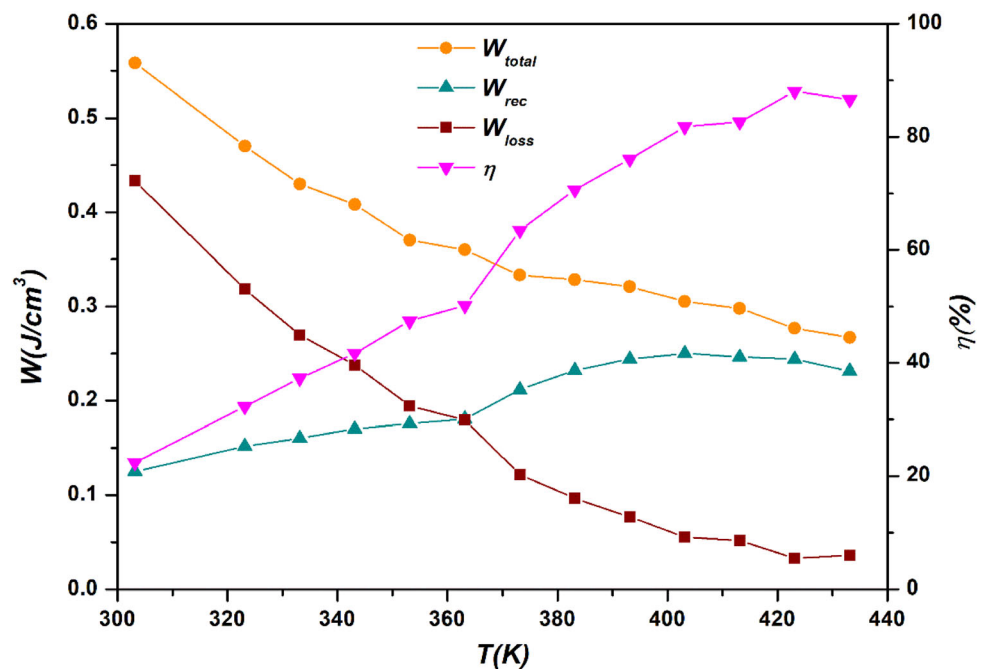
0.43 J/cm³ respectively, with the increasing applied electric field from 5 to 55 kV/cm. However, the value of η increases steadily with increasing the electric field. From 5 to 55 kV/cm, η increased from 15.10 to 24.12%. These results indicate that higher applied electric fields can induce more polarization, enhancing the energy storage properties [38].

### 3.6 Temperature-dependent energy storage properties

Another essential aspect of energy storage applications is the high-temperature stability of dielectric ceramics. To gain insight, the temperature dependence of energy storage properties of BCZT ceramic has been studied. Figure 7 shows the variation of

Table 2 Comparison of energy storage properties of BCZT ceramic with other lead-free materials from the literature

Sample	Method	T of sintering	ε'_r	W_{rec} (J/cm³)	η (%)	E (kV/cm)	T (K)	References
$Ba_{0.85}Ca_{0.15}Zr_{0.1}Ti_{0.9}O_3$	Sol–gel	1420	17,658	0.07	27.43	27	RT	This work
$Ba_{0.85}Ca_{0.15}Zr_{0.1}Ti_{0.9}O_3$	Sol–gel	1420	17,658	0.12	24.12	55	RT	This work
$Ba_{0.85}Ca_{0.15}Zr_{0.1}Ti_{0.9}O_3$	Sol–gel	1420	17,658	0.24	88.05	55	324	This work
$Ba_{0.85}Ca_{0.15}Zr_{0.1}Ti_{0.9}O_3$	Sol–gel	1420	16,310	0.01	63.65	7.77	413	[16]
$Ba_{0.85}Ca_{0.15}Zr_{0.1}Ti_{0.9}O_3$	Solid-state	1500	19,277	0.06	87.4	20	373	[40]
$Ba_{0.85}Ca_{0.15}Zr_{0.1}Ti_{0.9}O_3$	Solid-state	1350	16,200	0.12	51.3	60	303	[42]
$Ba_{0.85}Ca_{0.15}Zr_{0.1}Ti_{0.9}O_3$	Hydrothermal	1250	5000	0.41	78.6	60	380	[41]
$Ba_{0.85}Ca_{0.15}Zr_{0.1}Ti_{0.9}O_3$	Coprecipitation	1440	–	0.54	71	150	–	[43]
$BTSn_{0.11}$	Solid-state	1350	17,390	0.08	91.04	25	333	[44]
$BaZr_{0.05}Ti_{0.95}O_3$	High energy ball milling	1200	1300	0.10	56	30	RT	[10]
$BaZr_{0.05}Ti_{0.95}O_3$	High energy ball milling	1200	1300	0.218	72	50	RT	[10]

ε'_r: Dielectric constant, W_{rec}: recoverable energy density, η: efficiency coefficient, E: electric field
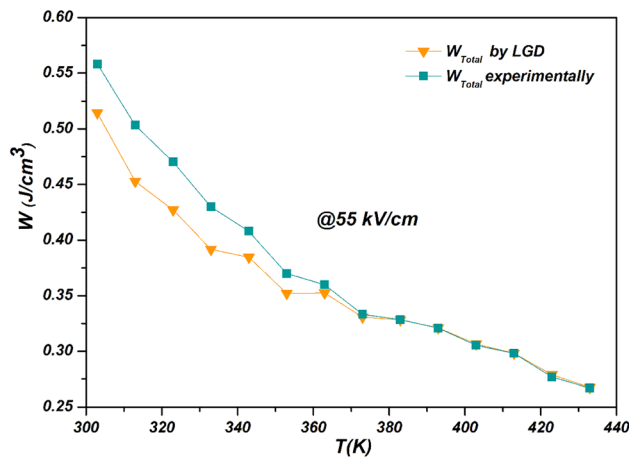
Fig. 8 Comparison of the thermal evolution of W_{total} obtained experimentally and using Landau–Ginzburg–Devonshire (LGD) theory at 55 kV/cm for BCZT ceramic

W_{total}, W_{rec}, W_{loss}, and η for BCZT ceramic as a function of temperature. On the one hand, W_{rec} increase with the increase in temperature. This behavior may be due to the enhancement in the mobility of domain walls with a rise in temperature [38]. On the other hand, a decrease in W_{loss} values with increased temperature is observed. This behavior can be attributed to ease in the reorientation of domains with rising temperature [39]. As a result, energy storage efficiency is enhanced. At the maximum electric field of 55 kV/cm, the maximum efficiency value is $\eta = 88.05\%$ at 324 K with $W_{rec} = 0.24$ J/cm³. These results are comparable to others reported in the

literature under a different electric field (Table 2). Using the same synthesis method and the temperature of synthesis, Mezzourh et al. [16] found a recovered energy density W_{rec} of 0.02 J/cm³ and storage efficiency η of 63.65% under 7.7 kV/cm in BCZT ceramic. On the other hand, by using an electric field of 20 kV/cm, Cai et al. [40] reported a recovered energy density of 0.06 J/cm³ and storage efficiency of 85.8% in BCZT ceramic elaborated by the solid-state method with almost the same grain size (44.37 μm) as our samples, which is lower than our results. For BCZT synthesis by sol–gel hydrothermal and at 60 kV/cm, the obtained W_{rec} was 0.36 J/cm³ and η = 67.25% with the grain size of 22.1 μm, as stated by Hanani et al. [41].

In comparison, BCZT ceramic under 55 kV/cm exhibited lower energy storage performances. Therefore, it is important to note that the energy-storage properties depend on the method of synthesis as well as the grain size. The better energy density may be due to smaller grain sizes and more uniform grain microstructure.

3.7 Temperature-dependent energy storage density using landau phenomenological approach

More insight into calculations of the total energy density W_{total} can be obtained based on the Landau–Ginzburg–Devonshire (LGD) phenomenological theory, describing the macroscopic phenomena in

ferroelectric materials near the phase transition. The total energy density W_{total} can be calculated by considering the simple Landau-type free energy model [48]:

$$F = F_0 + aP^2 + bP^4 + cP^6 - EP \qquad (5)$$

where a, b and c are the temperature-dependent coefficients. In ferroelectrics, $a(T) = a_1(T - T_c)$ where T_c is the curie temperature. At equilibrium, the first deviation of free energy should equal zero ($\partial F/\partial P = 0$) [45], which thus leads to:

$$E = aP + bP^3 cP^5 \qquad (6)$$

The electric field versus polarization (E–P) data for all considered temperatures can be fitted by Eq. (6), which allows the extraction of the a, b and c parameters for each temperature. These coefficients are important for energy storage because they express the energy density, according to the Landau model [45], where P_{max} is the polarization at E_{max}.

$$\begin{aligned} W_{total} &= \int_0^{P_{max}} (aP + bP^3 + cP^5) dP \\ &= \frac{1}{2} aP_{max}^2 + \frac{1}{4} bP_{max}^4 + \frac{1}{6} cP_{max}^6 \end{aligned} \qquad (7)$$

Figure 8 compare the temperature-dependence of the estimated W_{total} obtained via LGD theory with that deduced from the experimental results under 55 kV/cm in BCZT ceramic. Both methods show the same trend, W_{total} decreases with increasing temperature. At room temperature, the W_{total} obtained by LGD was 0.51 J/cm^3, which is lower than that found experimentally (0.55 J/cm^3). However, both methods lead to the same values at the paraelectric phase transition. Note, the coefficients a, b and c are temperature-dependent in relaxor ferroelectrics, which could be the main reason for the difference between the results obtained by the theoretical calculation and the experimental result [46].

3.8 Indirect electrocaloric measurements

The electrocaloric effect (ECE) is universally known as the reversible entropy and temperature change when an electric field is applied or removed [47]. An indirect method based on Maxwell's relation between the entropy (S) and the dielectric polarization (P) is used to estimate the adiabatic temperature change ΔT [48]:

$$\left(\frac{\partial P}{\partial T}\right)_E = \left(\frac{\partial S}{\partial E}\right)_T \qquad (8)$$

ΔT under an applied electric field is calculated by the following equation:

$$\Delta T = -\frac{1}{\rho} \int_{E_1}^{E_2} \frac{T}{C_P} \left(\frac{\partial P}{\partial T}\right)_E dE \qquad (9)$$

where P is polarization, ρ is the density of the sample, and C_P denotes the specific heat capacity of the material. E_1 and E_2 are initial and final applied electric fields, respectively. E_1 is taken as zero in the present case and E_2 corresponds to the saturation field value. The value of polarization gradient $(\partial P/\partial T)_E$ was found from the derivation of P versus T data [39].

Temperature change alone does not provide sufficient data to determine the global EC performance. Thus, the isothermal entropy change (ΔS) is an important parameter to evaluate the relative heat extraction capacity of the material. ΔS is calculated by the following equation:

$$\Delta S = -\frac{1}{\rho} \int_{E_1}^{E_2} \left(\frac{\partial P}{\partial T}\right)_E dE \qquad (10)$$

Figure 9a, b shows the variation of ΔT and ΔS as a function of temperature at different applied electric fields for BCZT ceramic. It has been observed that ΔT and ΔS increase with the increase in the electric field. This behavior is as per Eqs. (9) and (10). ΔT and ΔS curves, which correspond to a fixed applied electric field, exhibit a maximum around T_c due to the diffusion behavior of our sample near the ferroelectric-to-paraelectric phase transition and multiphase coexistence [49]. From Eqs. (9) and (10), it is evident that materials having a more significant polarization gradient as well as a higher saturation field (E_2) will show larger ΔT. At ΔE_{max} of 55 kV/cm, ΔT_{max} was 2.32 K, and ΔS_{max} was 1.98 J/Kg/K for BCZT ceramic with a thickness of 400 μm. The maximum peak is near transition temperature for lower electric fields. However, the peak position of ΔT_{max} and ΔS_{max} moves gradually toward the higher temperature with increasing the intensity of the applied electric field. This peak shift relates to the diffused nature of phase transition, which might be due to a change in domain configuration or field-induced
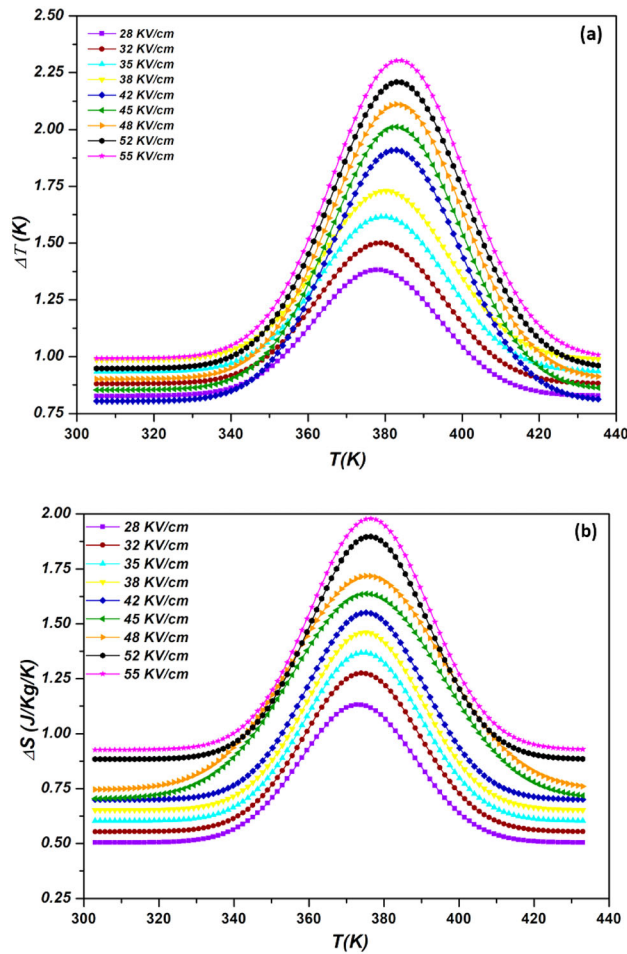
Fig. 9 **a** Temperature profiles of the electrocaloric temperature change (ΔT) at various applied electric fields, **b** temperature profiles of the isothermal entropy change (ΔS) at various applied electric fields

transition on the application of higher electric fields [38].

However, comprehensive conclusions cannot be drawn alone with adiabatic temperature change (ΔT) values about the overall caloric performance of a ferroelectric material. Thus, the electrocaloric responsivity ($\Delta T/\Delta E$), i.e., the ratio of adiabatic temperature change and the field change, is an important parameter to evaluate the ECE behavior of the material [50]. At 384 K, the maximum electrocaloric responsivity ζ_{max} is 0.42 K mm/kV at 55 kV/cm for BCZT ceramic. The EC effect compared for different materials, electric fields, and thickness are gathered in (Table 3). We can observe that the same material with the same composition shows different ECE. Certainly, for the BCZT with 1 mm of thickness and synthesized by solid-state, ζ_{max} reached 0.23 K mm/kV at 25 kV/cm [32], which is lower than our results. On the other hand, with the same ceramic thickness of 1 mm, the ECE of BCZT at 27 kV/cm was higher than many other lead-free ceramics. Indeed, Patel et al. [34] elaborated the $(Ba_{0.85}Ca_{0.15})(Zr_{0.1}Ti_{0.88}Sn_{0.02})O_3$ ceramics by solid oxide reaction, revealing that the ECE response reached high values of 0.84 K and 0.26 K mm/kV for ΔT_{max} and ζ_{max}, respectively, under 32 kV/cm at 347 K. As well as $(Ba_{0.85}Sr_{0.15})(Zr_{0.1}Ti_{0.9})O_3$ ceramics fabricated by conventional solid-state reaction route, which $\Delta T_{max} = 0.5$ K and $\zeta_{max} = 0.16$ K mm/kV at 347 K at 30 kV/cm, as stated by Patel et al. [51]. At an electric field of 55 kV/cm, BCZT exhibited better ECE properties compared to those found in $0.98(BaTiO_3)$–

Table 3 Comparison of the ECE properties of BCZT ceramic with other lead-free materials from the literature

Materials	T (K)	ΔT (K)	ΔE (kV/cm)	ζ_{max} (K mm/kV)	Thickness (mm)	RC (J/kg)	COP	References
$Ba_{0.85}Ca_{0.15}Zr_{0.1}Ti_{0.9}O_3$	384	2.32	55	0.42	0.4	4.59	12.38	This work
$Ba_{0.85}Ca_{0.15}Zr_{0.1}Ti_{0.9}O_3$	367	1.47	60	0.24	0.34	2.38	–	[41]
$(Ba_{0.85}Ca_{0.15})(Zr_{0.1}Ti_{0.88}Sn_{0.02})O_3$	353	0.84	32	0.26	1	–	–	[34]
$(Ba_{0.85}Ca_{0.075}Sr_{0.075})(Zr_{0.1}Ti_{0.88}Sn_{0.02})O_3$	305	1.5	33	0.455	1	2.75	–	[35]
$(Ba_{0.85}Sr_{0.15})(Zr_{0.1}Ti_{0.9})O_3$	347	0.5	30	0.16	1	–	–	[51]
$0.98(BaTiO_3)$–$0.02\ Bi(Mg_{0.5}Ti_{0.5})O_3$	416	1.21	55	0.22	2	1.47	–	[52]
$Ba_{0.85}Ca_{0.15}Zr_{0.1}Ti_{0.9}O_3$	373	0.57	25	0.23	1	0.35	11	[53]
$0.45(Ba_{0.2}Ti_{0.8}O_3)0.55(Ba_{0.7}Ca_{0.3}TiO_3)$	404	0.46	12	0.38	0.75	–	–	[57]
$Ba_{0.4}Sr_{0.6}Nb_2O_6$	407	0.32	60	0.05	0.6	–	–	[58]
$0.9(K_{0.5}N_{a0.5})NbO_3$–$0.1(SrZrO_3)$	367	1.19	35	0.34	1	–	0.62	[59]
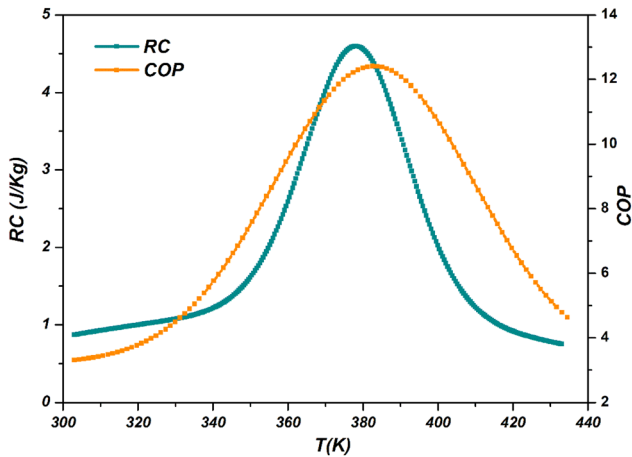
Fig. 10 Temperature profiles of refrigeration capacity (RC) and the coefficient of performance (COP) at 55 kV/cm for BCZT ceramic

0.02 $Bi(Mg_{0.5} Ti_{0.5})O_3$ ceramics with 2 mm of a thickness ($\Delta T_{max} = 1.21$ K and $\zeta_{max} = 0.22$ K mm/kV at 416 K) by Li et al. [52]. The synthesis conditions (such as calcination and sintering), chemical doping, grain form, the number of coexisting phases, the ceramic thickness, and the applied external electric field are all factors that contribute to these differences.

It is crucial to remember that measurements' frequency and temperature interval can affect the ECE values derived from indirect measurements utilizing PE hysteresis loops. It can also be affected by C_p, which is, in approximation, held constant. For that reason, refrigeration capacity (RC) is evaluated to look at the overall material's performance. RC is calculated by the following equation:

$$RC = \Delta T \times \Delta S \tag{11}$$

Figure 10 shows the variation of *RC* as a function of temperature at 55 kV/cm for BCZT ceramic. *RC* increases with increasing electric field. RC shows a maximum around T_c due to phase transition, as discussed before. At 55 kV/cm, RC_{max} was estimated to be 4.59 J/kg for BCZT with a thickness of 400 μm. The obtained value was higher than many other lead-free ceramics [35, 52].

Another important measure in evaluating the EC performance is the coefficient of performance (COP) as calculated by the following equation, where Q is the isothermal heat.

$$COP = \left| \frac{Q}{W_{total}} \right| = \left| \frac{T\Delta S}{W_{total}} \right| \tag{12}$$

Figure 10 displays the variation of COP as a function of temperature at 55 kV/cm for BCZT ceramic. The COP reveals the same behaviors as ΔT, ΔS and *RC*. Around T_c, *COP* exhibits a maximum. At 55 kV/cm, COP_{max} was 12.38 for BCZT ceramic. The obtained value is higher than that obtained by other literature [41, 53]. Nanocrystalline ceramics of [$(k_{0.5}na_{0.5})nbo_3]_{0.97}$-[lisbo_3]_{0.03}$ show a COP of 8.14 under an electric field of 40 kV/cm as reported by Kumar et al. [54]. Whereas Hao et al. [55] report a COP of 2.9 in $Pb_{0.97}La_{0.02}Zr_{0.87}Sn_{0.08}Ti_{0.07}O_3$ antiferroelectric thick film. Attending a strong electric field by reducing the thickness of ceramics can improve the EC parameters. The high values of ΔT, ΔS, ζ, RC and COP make BCZT ceramic with low thickness a promising candidate for eco-friendly electrocaloric applications.

The temperature change, ΔT, can also be calculated using Landau–Ginzburg–Devonshire phenomenological theory. The free energy can be definite as Eq. (5) in terms of electric polarization. The entropy change is obtained from Eq. (13) [56].

$$\Delta S = -\left(\frac{\partial F}{\partial T}\right)_E$$
$$= -\left(\frac{1}{2}a_1(T + \Delta T)P^2(E, T + \Delta T) - \frac{1}{2}a_1(T)P^2(0, T)\right) \tag{13}$$

The EC response can be given using $\Delta T = -(T\Delta S/C_p)$ [56] as follows:

$$\Delta T = -\left(\frac{T\Delta S}{C_p}\right)$$
$$= -\frac{T}{2C_p}(a_1(T + \Delta T)P^2(E, T + \Delta T)$$
$$- a_1(T)P^2(0, T)) \tag{14}$$

where C_p is the specific heat capacity of the material at given field E. Since $\Delta T \ll T$, Eq. 14 can be simplified to:

$$\Delta T = -\frac{T}{2C_p}(a_1(T)P^2(E, T) - a_1(T)P^2(0, T)) \tag{15}$$

Figure 11 compare the temperature-dependence of the estimated ΔT obtained via LGD theory with that deduced from the experimental results under 55 kV/cm in BCZT ceramic. Both methods show the same
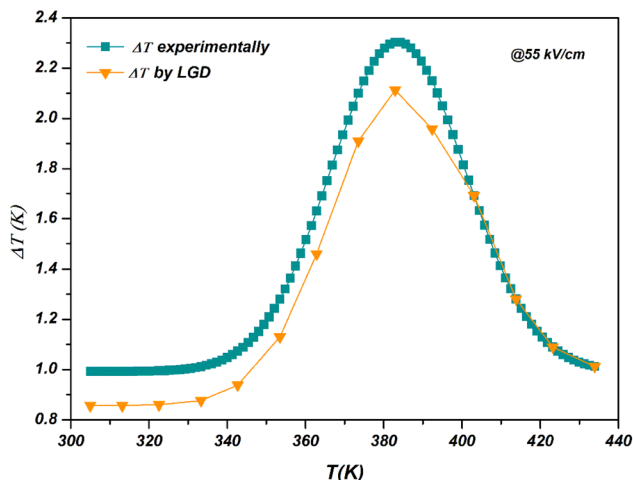
Fig. 11 Comparison of the thermal evolution of ΔT obtained by Landau–Ginzburg–Devonshire (LGD) theory and experimentally at 55 kV/cm for BCZT ceramic

behavior, ΔT increase with temperature increasing, reach a maximum around T_c, and then decrease. This comportment is due to the diffusion behavior of our sample near the ferroelectric-to-paraelectric phase transition [49], as discussed before. At room temperature, the ΔT obtained by LGD was 2.33 K, which is lower than that found experimentally (2.11 K). However, the same values at the paraelectric phase transition were observed for both methods. The difference between the results obtained by the theoretical calculation and the experimental result may be due to the coefficients a, b and c, which are temperature-dependent in relaxor ferroelectrics [56].

4 Conclusion

$Ba_{0.85}Ca_{0.15}Zr_{0.1}Ti_{0.9}O_3$ ceramic sintered at 1420 °C for 4 h was successfully prepared by the sol–gel method. The XRD showed the coexistence of two tetragonal and orthorhombic phases at room temperature. The SEM revealed a large grain size of ~ 45 μm. The ceramic thickness was reduced to achieve high-energy storage and a large electrocaloric effect in bulk ceramics. The BCZT ceramic with a thickness of 400 μm showed both interesting energy storage properties and a significant electrocaloric effect. The recoverable energy density W_{rec} was 0.24 J/cm^3, and W_{total} was 0.27 J/cm^3 with an efficiency coefficient of $\sim 88\%$ at 423 K under a 55 kV/cm electric field. On the other hand, BCZT show an outstanding

temperature change $\Delta T = 2.32$ K and significant electrocaloric responsivity $\zeta = 0.421$ K mm/kV, high refrigeration capacity RC = 4.59 J/kg and interesting coefficient of performance COP = 12.38. The total energy density W_{total} and the temperature change ΔT were also calculated by exploiting the Landau-Ginzburg-Devonshire (LGD) theory. The theoretical result matched the experimental findings. These characteristics suggest that this eco-friendly BCZT ceramic could be a prospective candidate for dielectric energy storage and electrocaloric applications.

Author contributions

All authors certify that they have participated sufficiently in the work to take public responsibility for the content. Furthermore, each author certifies that this work has not been and will not be submitted to other journal or published in any other publication before. AL: investigation, methodology, data curation, writing original draft, validation. HM: investigation, methodology, validation. DM: visualization, methodology, writing—review & editing, validation, supervision. MA: formal analysis, validation. LH: visualization, review, editing, validation, supervision. EHC: visualization, review, editing, validation, supervision. IAL: formal analysis, validation. ZK: review & editing, visualization, validation. MEM: visualization, writing—review & editing, validation, supervision. On behalf of all co-authors.

Data availability

Not applicable.

Code availability

Not applicable.

Declarations

Conflict of interest   Not applicable.

Ethical approval   Not applicable.

Consent to participate   We confirm that all authors mentioned in the manuscript have participated in, read and approved the manuscript, and have given their consent for the submission and subsequent publication of the manuscript.

Consent for publication   We confirm that all the authors mentioned in the manuscript have agreed to publish this paper.

Relevance summary   In this study, we report the successful preparation of lead-free $Ba_{0.85}Ca_{0.15}Zr_{0.1-}Ti_{0.9}O_3$ ceramic with reduced thickness to reach a high electric field. The study of their structural, dielectric, and ferroelectric properties were also reported. The energy storage and electrocaloric properties were investigated using the indirect experimental approach based on the Maxwell relation and the Landau-Ginzburg-Devonshire (LGD) theory. We confirm that this work is original and has not been published elsewhere, nor it is not currently under consideration for publication elsewhere.

References

1. Y. Xu, *Ferroelectric materials and their applications* (Elsevier, New York, 2013)

2. R.E. Cohen, Origin of ferroelectricity in perovskite oxides. Nature **358**(6382), 136–138 (1992). https://doi.org/10.1038/358136a0

3. S. Zhang, F. Li, High performance ferroelectric relaxor-$PbTiO_3$ single crystals: Status and perspective. J. Appl. Phys. **111**(3), 031301 (2012). https://doi.org/10.1063/1.3679521

4. L. Wu, C.-C. Wei, T.-S. Wu, C.-C. Teng, Dielectric properties of modified PZT ceramics. J. Phys. C: Solid State Phys. **16**(14), 2803–2812 (1983). https://doi.org/10.1088/0022-3719/16/14/020

5. H.-B. Park, C.Y. Park, Y.-S. Hong, K. Kim, S.-J. Kim, Structural and dielectric properties of PLZT ceramics modified with lanthanide ions. J. Am. Ceram. Soc. **82**(1), 94–102 (1999). https://doi.org/10.1111/j.1151-2916.1999.tb01728.x

6. P.K. Panda, B. Sahoo, PZT to lead free piezo ceramics: a review. Ferroelectrics **474**(1), 128–143 (2015). https://doi.org/10.1080/00150193.2015.997146

7. Y. Huan, X. Wang, J. Fang, L. Li, Grain size effect on piezoelectric and ferroelectric properties of $BaTiO_3$ ceramics. J. Eur. Ceram. Soc. **34**(5), 1445–1448 (2014). https://doi.org/10.1016/j.jeurceramsoc.2013.11.030

8. K. Sakayori et al., Curie temperature of $BaTiO_3$. Jpn. J. Appl. Phys. **34**(9S), 5443 (1995). https://doi.org/10.1143/JJAP.34.5443

9. X.M. Chen, T. Wang, J. Li, Dielectric characteristics and their field dependence of $(Ba, Ca)TiO_3$ ceramics. Mater. Sci. Eng. B **113**(2), 117–120 (2004). https://doi.org/10.1016/j.mseb.2004.04.003

10. T. Badapanda, S. Chaterjee, A. Mishra, R. Ranjan, S. Anwar, Electric field induced strain, switching and energy storage behaviour of lead free Barium Zirconium Titanate ceramic. Physica B **521**, 264–269 (2017)

11. D. Xue, Y. Zhou, H. Bao, J. Gao, C. Zhou, X. Ren, Large piezoelectric effect in Pb-free Ba(Ti, Sn)O3–x(Ba, Ca)TiO3 ceramics. Appl. Phys. Lett. **99**(12), 122901 (2011). https://doi.org/10.1063/1.3640214

12. P. Julphunthong, S. Chootin, T. Bongkarn, Phase formation and electrical properties of $Ba(Zr_xTi_{1−x})O_3$ ceramics synthesized through a novel combustion technique. Ceram. Int. **39**, S415–S419 (2013). https://doi.org/10.1016/j.ceramint.2012.10.105

13. X.W. Wang et al., Effects of calcining temperature on structure and dielectric and ferroelectric properties of sol–gel synthesized $Ba_{0.85}Ca_{0.15}Zr_{0.1}Ti_{0.9}O_3$ ceramics. J. Electron. Mater. **49**(1), 880–887 (2020). https://doi.org/10.1007/s11664-019-07769-4

14. M.B. Abdessalem, S. Aydi, A. Aydi, N. Abdelmoula, Z. Sassi, H. Khemakhem, Polymorphic phase transition and morphotropic phase boundary in $Ba_{1−x}Ca_xTi_{1−y}Zr_yO_3$ ceramics. Appl. Phys. A **123**(9), 583 (2017). https://doi.org/10.1007/s00339-017-1196-7

15. W. Liu, X. Ren, Large piezoelectric effect in Pb-free ceramics. Phys. Rev. Lett. **103**(25), 257602 (2009). https://doi.org/10.1103/PhysRevLett.103.257602

16. H. Mezzourh et al., Enhancing the dielectric, electrocaloric and energy storage properties of lead-free $Ba_{0.85}Ca_{0.15}Zr_{0.1-}Ti_{0.9}O_3$ ceramics prepared via sol–gel process. Phys. B: Condens. Matter **603**, 412760 (2021)

17. Z. Wang et al., Synthesis, structure, dielectric, piezoelectric, and energy storage performance of $(Ba_{0.85}Ca_{0.15})(Ti_{0.9}Zr_{0.1})O_3$ ceramics prepared by different methods. J. Mater. Sci.: Mater. Electron. **27**(5), 5047–5058 (2016). https://doi.org/10.1007/s10854-016-4392-x

18. M. Maraj, W. Wei, B. Peng, W. Sun, Dielectric and energy storage properties of $Ba_{(1−x)}Ca_xZr_yTi_{(1−y)}O_3$ (BCZT): A Review. Materials **12**(21), 3641 (2019). https://doi.org/10.3390/ma12213641

19. Y. Zhang, H. Sun, W. Chen, A brief review of $Ba(Ti_{0.8−}Zr_{0.2})O_3$–$(Ba_{0.7}Ca_{0.3})TiO_3$ based lead-free piezoelectric ceramics: past, present and future perspectives. J. Phys. Chem. Solids **114**, 207–219 (2018). https://doi.org/10.1016/j.jpcs.2017.10.041

20. X. Ji et al., Structural and electrical properties of BCZT ceramics synthesized by sol–gel process. J. Mater Sci. (2018). https://doi.org/10.1007/s10854-018-8751-7

21. Y. Yao et al., Large piezoelectricity and dielectric permittivity in $BaTiO_{3−X}BaSnO_3$ system: the role of phase coexisting. Europhys. Lett. (EPL) (2012). https://doi.org/10.1209/0295-5075/98/27008

22. H. Kaddoussi et al., Indirect and direct electrocaloric measurements of $(Ba_{1−x}Ca_x)(Zr_{0.1}Ti_{0.9})O_3$ ceramics ($x = 0.05$, $x = 0.20$). J. Alloys Compd. **667**, 198–203 (2016). https://doi.org/10.1016/j.jallcom.2016.01.159

23. J. Li et al., Grain-orientation-engineered multilayer ceramic capacitors for energy storage applications. Nat. Mater. **19**(9), 999–1005 (2020). https://doi.org/10.1038/s41563-020-0704-x

24. C. Neusel, H. Jelitto, D. Schmidt, R. Janssen, F. Felten, G.A. Schneider, Thickness-dependence of the breakdown strength: analysis of the dielectric and mechanical failure. J. Eur. Ceram. Soc. **35**(1), 113–123 (2015). https://doi.org/10.1016/j.jeurceramsoc.2014.08.028

25. I. Coondoo, N. Panwar, H. Amorín, M. Alguero, A.L. Kholkin, Synthesis and characterization of lead-free $0.5Ba(Zr_{0.2}Ti_{0.8})O_3$–$0.5(Ba_{0.7}Ca_{0.3})TiO_3$ ceramic. J. Appl. Phys. **113**(21), 214107 (2013)

26. P. Jaimeewong, M. Promsawat, A. Watcharapasorn, S. Jiansirisomboon, Comparative study of properties of BCZT ceramics prepared from conventional and sol-gel auto combustion powders. Integr. Ferroelectr. **175**(1), 25–32 (2016). https://doi.org/10.1080/10584587.2016.1199913

27. Y. Tian, L. Wei, X. Chao, Z. Liu, Z. Yang, Phase transition behavior and large piezoelectricity near the morphotropic phase boundary of lead-free free $(Ba_{0.85}Ca_{0.15})(Zr_{0.1}Ti_{0.9})O_3$ ceramics. J. Am Ceram. Soc. **96**(2), 496–502 (2013)

28. S. Belkhadir et al., Structural, dielectric and electrocaloric properties of $(Ba_{0.85}Ca_{0.15})(Ti_{0.9}Zr_{0.1−x}Sn_x)O_3$ ceramics elaborated by sol–gel method. J. Mater. Sci **30**(15), 14099–14111 (2019)

29. Z. Hanani et al., Enhanced dielectric and electrocaloric properties in lead-free rod-like BCZT ceramics. J. Adv. Ceram. **9**(2), 210–219 (2020)

30. E.K. Abdel-Khalek, D.A. Rayan, A.A. Askar, M.I.A.A. Maksoud, H.H. El-Bahnasawy, Synthesis and characterization of $SrFeO_{3−δ}$ nanoparticles as antimicrobial agent. J. Sol-Gel Sci. Technol. **97**(1), 27–38 (2021). https://doi.org/10.1007/s10971-020-05431-8

31. H. Kaddoussi et al., Room temperature electro-caloric effect in lead-free) $Ba(Zr_{0.1}Ti_{0.9})_1−SnO_3(x = 0, x = 0.075)$ ceramics. Solid State Commun. **201**, 64–67 (2015). https://doi.org/10.1016/j.ssc.2014.10.003

32. S. Merselmiz et al., Enhanced electrical properties and large electrocaloric effect in lead-free $Ba_{0.8}Ca_{0.2}Zr_xTi_{1−x}O_3$ ($x= 0$ and 0.02) ceramics. J. Mater. Sci **31**(19), 17018–17028 (2020)

33. M. Ben Abdessalem, I. Kriaa, A. Aydi, N. Abdelmoula, Large electrocaloric effect in lead-free $Ba_{1−x}Ca_xTi_{1−y}Zr_yO_3$ ceramics under strong electric field at room-temperature. Ceram. Int. **44**(12), 13595–13601 (2018)

34. S. Patel Sharma, R. Vaish, Enhanced electrocaloric effect $Ba_{0.85}Ca_{0.15}Zr_{0.1}Ti_{0.9−x}Sn_xO_3$ in ferroelectric ceramics. Phase Transit. **89**(11), 1062–1073 (2016)

35. S. Patel, M. Kumar, Electrocaloric properties of Sr and Sn doped BCZT lead-free ceramics. Eur. Phys. J. Appl. Phys. **91**(2), 20905 (2020). https://doi.org/10.1051/epjap/2020200165

36. Q. Zhang et al., Enhanced piezoelectric response of (Ba, Ca)(Ti, Zr) O3 ceramics by super large grain size and construction of phase boundary. J. Alloy. Compd. **794**, 542–552 (2019)

37. N. Qu, H. Du, X. Hao, A new strategy to realize high comprehensive energy storage properties in lead-free bulk ceramics. J. Mater. Chem. C **7**(26), 7993–8002 (2019). https://doi.org/10.1039/C9TC02088H

38. P. Redhu, A. Hooda Sharma, S. Dahiya, R. Punia, R.P. Tandon, Study of energy storage and electrocaloric behavior of lead-free Fe-doped BCT ceramics. Ferroelectrics **569**(1), 136–147 (2020). https://doi.org/10.1080/00150193.2020.1791661

39. K.R. Kandula, K. Banerjee, S.S.K. Raavi, S. Asthana, Enhanced electrocaloric effect and energy storage density of Nd-substituted 0.92 NBT-0.08 BT lead free ceramic. Phys. Status Solidi (a) **215**(7), 1700915 (2018)

40. W. Cai et al., Synergistic effect of grain size and phase boundary on energy storage performance and electric properties of BCZT ceramics. J. Mater. Sci.: Mater. Electron. **31**(12), 9167–9175 (2020)

41. Z. Hanani et al., Thermally-stable high energy storage performances and large electrocaloric effect over a broad

temperature span in lead-free BCZT ceramic. RSC Adv. **10**(51), 30746–30755 (2020)

42. K. Xu Yang, W. Peng, L. Li, Temperature-stable MgO-doped BCZT lead-free ceramics with ultra-high energy storage efficiency. J. Alloys Compd. **829**, 154516 (2020)

43. Q. Zhang et al., Controllable synthesis of $(Ba_{0.85}Ca_{0.15})(Zr_{0.1}Ti_{0.9})O_3$ submicron sphere by hydroxide co-precipitation method. Ceram. Int. **46**(18), 28285–28291 (2020). https://doi.org/10.1016/j.ceramint.2020.07.331

44. S. Merselmiz et al., High energy storage efficiency and large electrocaloric effect in lead-free $BaTi_{0.89}Sn_{0.11}O_3$ ceramic. Ceram. Int. **46**(15), 23867–23876 (2020). https://doi.org/10.1016/j.ceramint.2020.06.163

45. Z. Jiang, S. Prosandeev, L. Bellaiche, Energy storage in lead-free $Ba(Zr, Ti)O_3$ relaxor ferroelectrics: Large densities and efficiencies and their origins. Phys. Rev. B **105**(2), 024102 (2022). https://doi.org/10.1103/PhysRevB.105.024102

46. Y. Hou, J. Li, J. Ding, T. Ye, R. Liang, Giant electrocaloric response in compositional manipulated $BaTiO_3$ relaxor–ferroelectric system. J. Appl. Phys. **127**(6), 064103 (2020). https://doi.org/10.1063/1.5142635

47. A.S. Mischenko, Q. Zhang, J.F. Scott, R.W. Whatmore, N.D. Mathur, Giant electrocaloric effect in thin-film $PbZr_{0.95}Ti_{0.05}O_3$. Science **311**(5765), 1270–1271 (2006). https://doi.org/10.1126/science.1123811

48. Z. Kutnjak, B. Rožič, R. Pirc, Electrocaloric effect: theory, measurements, and applications, in *Wiley Encyclopedia of Electrical and Electronics Engineering*. ed. by J.G. Webster (Wiley, Hoboken, 2015), pp. 1–19. https://doi.org/10.1002/047134608X.W8244

49. B. Zhang et al., Enhanced electrocaloric effect in the Sm and Hf co-doped $BaTiO_3$ ceramics. Ceram. Int. **47**(1), 1101–1108 (2021). https://doi.org/10.1016/j.ceramint.2020.08.226

50. Y. Liu, J.F. Scott, B. Dkhil, Direct and indirect measurements on electrocaloric effect: recent developments and perspectives. Appl. Phys. Rev. **3**(3), 031102 (2016). https://doi.org/10.1063/1.4958327

51. S. Patel, A. Chauhan, R. Vaish, Caloric effects in bulk lead-free ferroelectric ceramics for solid-state refrigeration. Energ. Technol. **4**(2), 244–248 (2016)

52. M.-D. Li, X.-G. Tang, S.-M. Zeng, Q.-X. Liu, Y.-P. Jiang, W.-H. Li, Giant electrocaloric effect in $BaTiO_3$–$Bi(Mg_{1/2}Ti_{1/2})O_3$ lead-free ferroelectric ceramics. J. Alloys Compd. (2018). https://doi.org/10.1016/j.jallcom.2018.03.102

53. S. Merselmiz et al., Thermal-stability of the enhanced piezoelectric, energy storage and electrocaloric properties of a lead-free BCZT ceramic. RSC Adv. **11**(16), 9459–9468 (2021). https://doi.org/10.1039/D0RA09707A

54. R. Kumar, S. Singh, Giant electrocaloric and energy storage performance of $[(K_{0.5}Na_{0.5})NbO_3]_{(1-x)}$–$[LiSbO_3]_x$ nanocrystalline ceramics. Sci Rep **8**(1), 3186 (2018). https://doi.org/10.1038/s41598-018-21305-0

55. X. Hao, Y. Zhao, Q. Zhang, Phase structure tuned electrocaloric effect and pyroelectric energy harvesting performance of $(Pb_{0.97}La_{0.02})(Zr,Sn,Ti)O_3$ antiferroelectric thick films. J. Phys. Chem. C **119**(33), 18877–18885 (2015). https://doi.org/10.1021/acs.jpcc.5b04178

56. R. Pirc, Z. Kutnjak, R. Blinc, Q.M. Zhang, Electrocaloric effect in relaxor ferroelectrics. J. Appl. Phys. **110**(7), 074113 (2011). https://doi.org/10.1063/1.3650906

57. G. Singh et al., Electro-caloric effect in $0.45BaZr_{0.2}Ti_{0.8}O_3$–$0.55Ba_{0.7}Ca_{0.3}TiO_3$ single crystal. Appl. Phys. Lett. **102**(8), 082902 (2013). https://doi.org/10.1063/1.4793213

58. H. Tang, X.-G. Tang, M.-D. Li, Q.-X. Liu, Y.-P. Jiang, Pyroelectric energy harvesting capabilities and electrocaloric effect in lead-free Sr Ba1-Nb2O6 ferroelectric ceramics. J. Alloys Compd. **791**, 1038–1045 (2019). https://doi.org/10.1016/j.jallcom.2019.03.385

59. R. Kumar, S. Singh, Enhanced electrocaloric response and high energy-storage properties in lead-free $(1-x)(K_{0.5}Na_{0.5})NbO_{3-x}SrZrO_3$ nanocrystalline ceramics. J. Alloys Compd. **764**, 289–294 (2018). https://doi.org/10.1016/j.jallcom.2018.06.083